A FINITE ELEMENT MODEL OF A SØDERBERG ELECTRODE WITH AN APPLICATION IN CASING DESIGN

I. Mc Dougall[1], C.F.R. Smith[2], B. Olmstead[1] and W.A. Gericke[3]

[1]CSIR, Private Bag X28, Auckland Park, 2006, RSA. E-mail: imcdougall@csir.co.za, bolmst@csir.co.za
[2]Samancor Manganese, Meyerton Works, P O Box 66, Meyerton, 1960, RSA. E-mail: clem.smith@samancor.co.za
[3]Xstrata SA (Pty) Ltd, Private Bag 82288, Rustenburg, 0300. E-mail: willieg@xstratasa.co.za

ABSTRACT

A finite element model was generated of a Søderberg electrode in a ferromanganese smelter. In this model, the casing and fins were modelled explicitly, and temperature-dependent material properties were included. A two-stage analysis procedure was used, the first part being a coupled thermal-electrical analysis using an applied DC current. As the casing material was non–magnetic, the DC current was deemed sufficiently accurate for this initial analysis. The proximity effect was not considered. Thermal boundary conditions based on assumed temperature distributions in the furnace were applied. Calculated temperatures agreed well with measured values. The joule heat calculated in this step was applied as a load to a coupled thermal-stress analysis.

The model was applied to a comparative study of alternative materials for the casing and fins. A number of different combinations of materials for the casing and fins were evaluated in a comparative study. The position of the baking zone was used as the criterion for evaluating the potential of each material combination. Based on this analysis, some material combinations were discarded as being entirely unsuitable, whilst the two most suitable combinations will be tested experimentally in the furnace. The stress analysis was performed on the most suitable option.

The practical advantage of this analysis was that a number of what-if scenarios could be evaluated and discarded prior to embarking on expensive experimental work, thus limiting the amount of experimental effort required. A mathematical model allows for the comparison of options under controlled conditions, where parameters of interest can be varied individually, with all other parameters remaining the same, a condition which is difficult to achieve in an operating furnace.

1. INTRODUCTION

Since the introduction of the Søderberg electrode during the 1920's, there has been an interest in understanding how it works. The first mathematical electrode models appeared in the 1970's. They were generally axisymmetric 2D models which used a finite difference technique to solve the appropriate thermal and electromagnetic equations. As computers became more sophisticated, the models became more complex, both in their geometry and in the physics which could be modelled. Finite element models were introduced by the mid–1980's. The electromagnetic descriptions as well as the boundary conditions have become more sophisticated as the field has advanced.

Much of the research in this field has been done at Elkem A/S in Norway, the company which patented the Søderberg Electrode. A number of researchers, notably Olsen[1,2,3,4] and Innvaer[1,2,3,4,5,6], have published extensively on that topic. Over a period of thirty years, a number of electrode models were been developed, which progressed from an axisymmetric two-dimensional model using DC current, to models simulating AC current [4], transient conditions [2] and stresses [4], and a model which calculated temperature and electrical current distributions in a segment of the electrode or in the entire electrode[5]. Jonsson and Ingason [7] describe a fully three-dimensional electrode model based on the earlier ELKEM models.

A number of other researchers have published descriptions of models, for example Arai and Ono [8,9]. Bullon, Bermudez et al [10,11,12,13,14] describe modelling work done to characterise the behaviour of compound graphite/Soderberg electrodes used in the smelting of silicon. Their models include an axisymmetric model, a transverse slice model and a three-dimensional model of the electrode. They calculate electromagnetic fields as well as current distributions, Joule heat fluxes, temperatures and stresses.

In a recently completed electrode modelling project, a finite element model of the Søderberg electrode was developed, which could be used to analyse a variety of scenarios. The available models included an AC electromagnetic model, a thermal model and a stress model, as well as a coupled thermal-electric model which simulates the application of a DC current.

In the current work, a finite element model was generated of the electrodes in one of the furnaces at the Samancor ferromanganese smelter in Meyerton. The purpose of this study was to determine whether the existing Grade 304 stainless steel casings and/or the fins could be replaced by a cheaper material such as Chromanite, 3CR12 or mild steel. 3Cr 12 and Chromanite are corrosion-resistant steels, 3Cr12 containing 12% Cr and 3% Ni, whilst Chromanite contains 18% Cr and 1% Ni. Chromanite is approximately 22% cheaper than, 304, and 3Cr 12 is a further 32% cheaper than Chromanite. A significant cost saving could be realised per annum by using either of these materials. A comparative study was conducted of a number of possible combinations of materials for casing and fins, all other parameters remaining equal. The material combinations under consideration are listed in Table 1. The criterion against which the materials were judged, was the position of the 450ºC isotherm. As a result of the high rate of consumption of the electrode, it is desirable that this isotherm be as high up in the contact shoe region as possible. The model was calibrated by comparing the position of the 450ºC isotherm with values measured previously at Meyerton for the existing Grade 304 casings and fins. Stresses were evaluated for the most promising option.

Table 1. Material Options Considered in the Analysis.

OPTION	CASING MATERIAL	FIN MATERIAL
1	Mild Steel	Mild Steel
2	304	304
3	Mild Steel	304
4	304	3CR12
5	304	Chromanite
6	304	Mild steel
7	3CR12	304
8	3CR12	3CR12
9	3CR12	Chromanite
10	3CR12	Mild Steel
11	Chromanite	304
12	Chromanite	3CR12
13	Chromanite	Chromanite
14	Chromanite	Mild Steel

2. ELECTRODE MODEL

The electrode is comprised of a number of components, notably the steel casing with fins and the carbon paste. Current is fed into the electrode by means of copper contact shoes, clamped to the electrode by means of a pressure ring. In addition, the electrode is supported by a holding arrangement which allows for “slipping” of the electrode. The electrode has a diameter of 1.9m. There are 16 fins of two radial lengths, ie 485mm and 325mm. The casing thickness is 4mm, whilst the fins are 3mm thick. The furnace has a 75MVA rating and a current of 144kA per phase.

In this study, the casing, fins and paste were modelled in detail. The contact shoes were modelled, but not in great detail, in order for the current transfer to the casing to be accurately simulated. The other auxiliaries, such as the holding arrangement, were not included in the model. The lower 6m of the electrode was modelled. This included the electrode from its lower tip to a position above the contact shoes, and was

sufficiently extensive to include the entire region of interest for this study. Due to limitations on the fineness of the mesh, it was not practicable to include the windows in the fins. The model is shown in Figures 1 and 2.

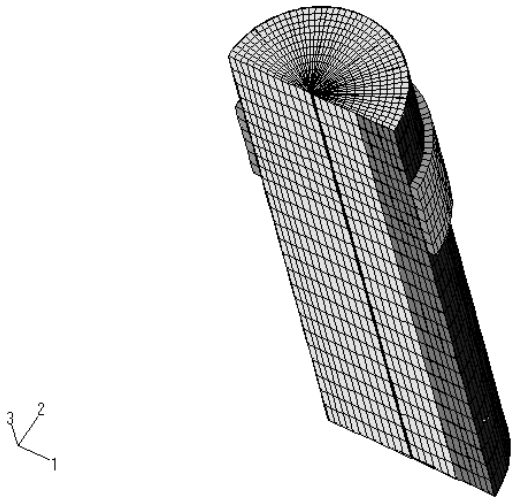

Figure 1. Complete Electrode Model.

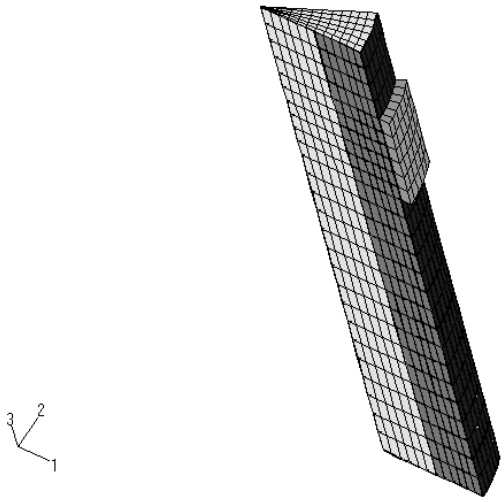

Figure 2. Single Segment of the Electrode.

The problem to be analysed is a coupled-field problem, which includes coupling of fluid dynamics, electromagnetics, thermal and structural physics. In the investigation under discussion, the fluid dynamics part of the problem is largely ignored; boundary conditions imposed on the electrode are based on the best available estimates.

The ABAQUS [16] finite element software was used to perform the analysis in two stages. A 180° segment of the electrode was included in this model. The first step was a steady-state coupled thermal-electric analysis, in which a DC electrical analysis was performed simultaneously with the thermal analysis. The analysis used 8-noded solid elements with two degrees of freedom, viz. temperature and voltage. The results obtained from the coupled thermal-electrical analysis included temperatures, electrical current density, electrical potential, electrical potential gradient, heat fluxes and Joule heat per element. Contact between the casing, fins and paste was included in this formulation. In ABAQUS contact is modelled by defining contact surfaces. An electrical conductivity and thermal conductivity across the gap were specified as a function of the gap size.

In the second step, the Joule heat obtained from the thermal-electric analysis, as well as radiation and convection boundary conditions, were used as the loading on the stress analysis. This analysis was performed as a coupled thermal-stress analysis, to allow for the accurate representation of the temperature-dependent nature of the materials. Contact between steel and carbon regions was included in this analysis. Eight-noded solid elements were used in the thermal–stress analysis. These elements had four nodal degrees of freedom, viz. u_x, u_y, u_z and temperature.

2.1 Material properties

The material properties required for the analysis include electrical conductivity, thermal conductivity, Young's modulus, Poisson ratio, yield strength, coefficient of thermal expansion and density for all the materials used.

Table 2. Material Properties of the Metals and Carbon.

Temperature [ºC]	Mild Steel	Grade 304 Stainless Steel	3CR12	Chromanite	Copper	Electrode Paste
Electrical Conductivity [$\Omega^{-1}.m^{-1}$]						
20	6.25×10^6	1.388×10^6	1.47×10^6	1.336×10^6	58.8×10^6	
100	4.54×10^6			1.176×10^6	41.7×10^6	0.1×10^6
						0.11×10^6
500	1.639×10^6	0.855×10^6		0.855×10^6	32.36×10^6	0.13×10^6
1000						0.17×10^6
1400						0.20×10^6
1800						0.25×10^6
2200						0.30×10^6
2600						0.38×10^6
Thermal Conductivity [$Wm^{-1}K^{-1}$]						
20	52.0	36.9		36.9	380.	
100	51.0	16.2	30.	32.2	370	
200						3.2
500	39.3	21.5	40.		300	6.8
1000						19.2
1400						30.3
1800						37.1
2200						40.2
2600						38.9
Young's Modulus [GPa]						
20	200	193	200	200	130	3.3
450						
Poisson Ratio						
constant	0.3	0.3	0.3	0.3	0.34	0.15
Linear Coeff. of Thermal Expansion [$m.m^{-1}K^{-1}$]						
0 –100	$17. \times 10^{-6}$	17.2×10^{-6}	11.1×10^{-6}	15.7×10^{-6}	$17. \times 10^{-6}$	
0 – 300	17.3×10^{-6}	17.8×10^{-6}	11.7×10^{-6}	17.3×10^{-6}	17.3×10^{-6}	
0 – 500	17.3×10^{-6}	18.4×10^{-6}	12.3×10^{-6}	18.7×10^{-6}	17.5×10^{-6}	
500 – 800						-11.6×10^{-6}
800 - 1000						-2.5×10^{-6}
1000 – 2500						4.3×10^{-6}
Density [kgm^{-3}]						
	7870	7900	7680	7810		1342
Yield Strength or 0.2% Proof Stress [MPa]						
Room Temp	300	205	280	450	450	17. (compressive)

The temperature-dependent nature of the material properties is one of the dominant causes of the difficulties in modelling the electrode. As the current enters the carbon paste at the contact shoe level, the resistive heating component causes the paste to melt and bake. During baking, the anthracite undergoes partial graphitization of the carbon accompanied by a loss of volatiles and solidification of the pitch binder. This results in an increase in both the electrical and thermal conductivities of the material. Baking occurs at a temperature of approximately 450°C. The shrinkage and subsequent expansion of the carbon during and after baking has a major effect on the integrity of the electrode. The carbon paste changes from being electrically and thermally non-conductive in its unbaked state, to being sufficiently conductive, both electrically and thermally, to perform the required duty as an electrode. Extensive work has been done to determine the material properties of the carbon. However, the results are considered proprietary. Typical material properties for the metals and paste obtained from the literature are included in Table 2. Thermal conductivity and electrical resistivity values for carbon paste were obtained from [11], whilst **c**oefficients of thermal expansion were quoted in [17] and mechanical properties in [18]

2.2 Thermal-Electric Analysis

Current is applied to the electrode through contact shoes clamped to the electrode to ensure good contact between the casing and electrode. Although the applied current to the electrode is actually AC, with two phases applied to each electrode, for this simulation the electrode is supplied with a DC current. Whilst it is known that the effect of the actual applied alternating current is to cause a concentration of the current near the surface of the electrode, it is believed that the DC analysis, being considerably simpler to perform, would be sufficiently accurate for this comparative study. The "skin effect" may safely be neglected in the steel casing and fins, as the material is thin and currents are high. The effect will be more pronounced in the carbon, although the relatively low electrical conductivity would lead to a significant "skin" thickness, of the order of several hundred millimetres.

2.2.1 Loads and Boundary Conditions

Electrical loads and boundary conditions were applied as a short circuit at the tip of the electrode (V=0) and a current of 144 000 amps on the contact shoes.

The thermal boundary conditions imposed on the model include both radiation and convection conditions on the portion of the electrode in contact with the furnace charge. The outer surface of the contact shoes, the casing above the contact shoes and the top surface of the model are kept at a constant temperature of 120˚C. This simulated the water cooling inside the contact shoes as well as the air cooled mantle surrounding the electrode above the contact shoes. The surface of the electrode below the contact shoes is subject to a varying temperature distribution. Both convective and radiative heat transfer occur on this surface. Metaxas [15] suggests that an electric arc such as is found in this system may be simulated by a radiation boundary condition. Consequently, the lower surface of the electrode is subject to radiation against an ambient temperature of 2500˚C, the assumed arc temperature.

The convective and radiative boundary conditions along the side of the electrode are based on a stepwise temperature distribution in the surrounding region, which decreases upwards, from the process temperature of 1380˚C at the base of the electrode to 260˚C at the base of the contact shoes. A film coefficient of 10 $W/m^2 K$ was used. An emissivity of 0.85 was used for the radiation.

The primary outputs of this stage of the analysis are the Joule heat flux calculated per element of the model and nodal temperatures.

2.3 Stress Analysis

The dominant cause of stress in the electrode is the differential thermal expansion in the casing and carbon. The ability of the electrode to resist stress is a function of the baking process. The baking of the carbon has a major effect on both its thermal and electrical conductivity and its coefficient of thermal expansion. As baking occurs in a relatively uncontrolled environment, it is difficult to predict exact values for the material properties of the baked material.

Under furnace conditions, the steel casing burns away above a temperature of about 1000˚C. This forces the current to pass into the carbon. This effect was included in the model by removing casing and fin elements with temperatures exceeding 1000˚C. The fin and casing configuration used for the stress analysis is shown in Figure 3.

The coupled thermal-stress analysis used 8-node solid elements, which have 4 degrees of freedom per node, being displacements in the x, y and z directions and temperature. Stresses, stress invariants and strains are derived from the displacements.

An important factor in the behaviour of the electrode is the state of contact between the casing and the paste. This has some implications for the conduction of electricity and heat between the two components. Contact surfaces were included at all the interfaces between the casing, fins and paste. The presence of a pressure ring which forces the contact shoes against the casing at all times precludes a loss of contact between these components. For the stress analysis, it was not deemed necessary to include the contact shoes in the model.

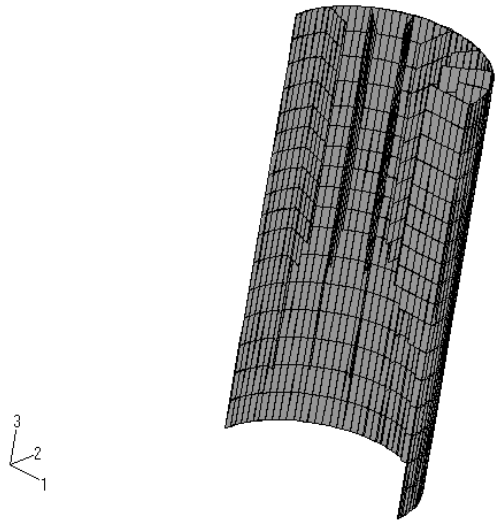

Figure 3. Casing and Fins as Used in Stress Analysis.

2.3.1 Loads and Boundary Conditions

It was necessary to fix the model against global translation and rotation in all three directions.

The full set of loads and boundary conditions are:

- the top of the electrode was restrained against vertical movement.
- two points on the symmetry (X_2=0) plane near the edge of the electrode (at the top surface) were restrained against lateral movement in the 1 direction
- all the points lying on the X_2=0 plane, which represented the symmetry plane through which the model was cut, were restrained against transverse movement in the 2 direction.
- the calculated Joule heating fluxes were imposed on all the elements of the carbon and casing.
- The radiative and convective boundary conditions imposed in the first stage of the analysis were imposed in this stage as well.

3. RESULTS

3.1 Thermal-Electric Analysis

The temperature field through the centre of the electrode in the X_2=0 plane in the contact shoe region for the existing configuration, namely 304 stainless steel casing and 304 fins, is depicted in Figure 4. As shown in Figure 1, there is a fin present on the right side of the electrode. Temperature values obtained from routine measurements on the furnace to monitor the position of the 450°C isotherm are superimposed on this figure. The correlation between measured and calculated values is fairly good. The electrode model did not account for the proximity of the other electrodes, which cause an asymmetry in the temperature field.

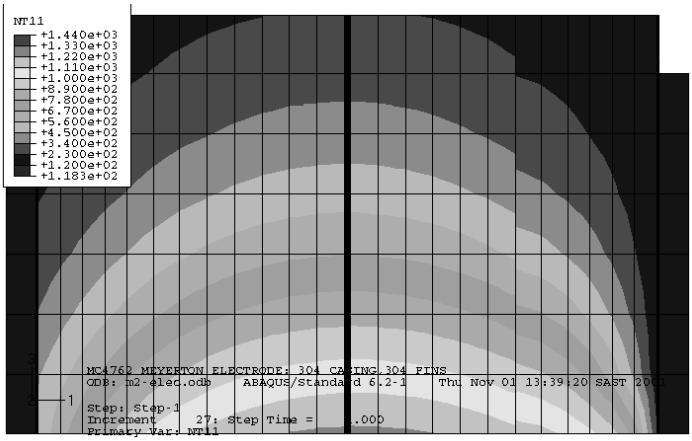

Figure 4. Temperature distribution in contact shoe area of existing electrode [°C]

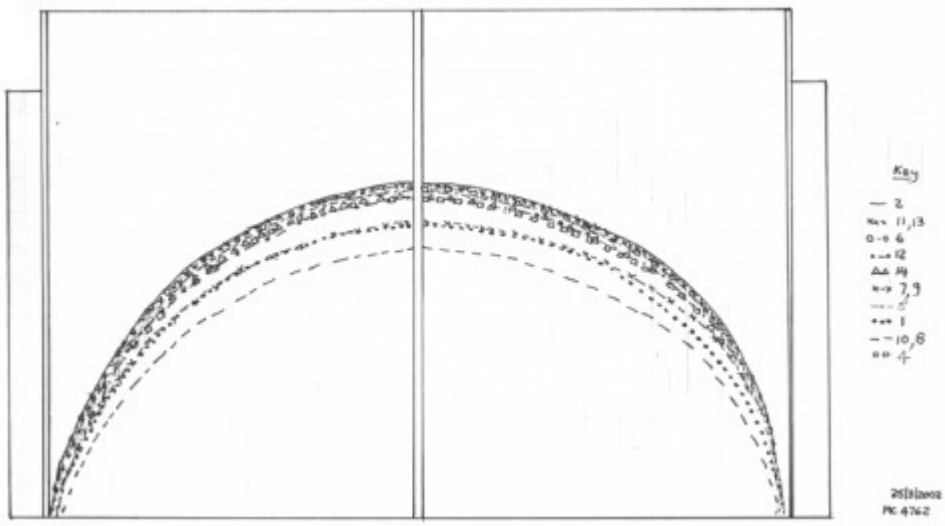

Figure 5. 450ºC Isotherm for the Different Material Options.

The position of the 450ºC isotherm is shown in Figure 5 for all the options. The small discontinuity observed on the right of the figure is due to the presence of a fin. It is interesting to note that the results tend to occur in groups. These groupings appear to be related primarily to the casing material, with the fin material having a secondary effect. It is also of interest to note that the all 304 case forms the upper bound, and therefore represents the most suitable configuration.

The material combinations may be arranged in order from the higher isotherms to the lower, as in Table 3. This ranking is based on the position of the isotherm in the carbon region, the isotherm in the fin being a secondary consideration. The most suitable substitute for the Grade 304 stainless steel casing and fins is the option which exhibits a 450ºC isotherm in a similar position to the existing configuration.

On the basis of these results, it may be suggested that a Chromanite casing with 304 fins or a Chromanite casing with Chromanite fins will perform as well as the current all-304 option. A 304 casing with mild steel fins performs almost as well. The use of Chromanite for both casing and fins may prove the most attractive option. It has the advantage that both casing and fins are manufactured from the same material, reducing possible difficulties in the welding of the two materials, as well as mismatches between thermal expansion coefficients.

Table 3. Ranking of Options according to position of the 450ºC isotherm.

RANKING	OPTION	Casing	Fins
(existing)	2	304	304
1	11	Chromanite	304
1	13	Chromanite	Chromanite
1	6	304	Mild Steel
1	5	304	Chromanite
2	14	Chromanite	Mild Steel
2	12	Chromanite	3CR12
2	4	304	3CR12
3	3	Mild Steel	304
4	7	3CR12	304
4	9	3CR12	Chromanite
4	1	Mild Steel	Mild Steel
5	10	3CR12	Mild Steel
5	8	3CR12	3CR12

3.2 Thermal-Stress Analysis

The configuration using Chromanite for both casing and fins was used for the thermal-stress analysis, as this appeared the most promising option. The maximum and minimum principal stresses in the carbon are depicted in Figures 6 and 7, whilst the equivalent Von Mises stresses in the steel are included as Figure 8. The asymmetry visible in Figures 6 and 7 is due to the presence of a fin at the right of the electrode, as may be seen in Figure 1.

The highest stresses in the steel occur at the base of the contact shoes. This is due to the steep thermal gradients in the steel at this level associated with the electric current, which enters the steel at this point, and causes resistive heating of the steel. In addition, the contact shoes are maintained at a constant temperature, which influences the surface temperature of the casing. The maximum values of the Von Mises stresses in the steel are of the order of 380 - 412MPa. Whilst these values are below the room temperature yield point of 450MPa, they may locally exceed the yield point at the ambient temperature. These maxima occur at the base of the contact shoes, at which level the electrode paste has baked, and the need for mechanical strength in the casing is no longer critical. The maximum principal stress in this region is in the order of 470MPa, with small peaks at the points of connection of the fins to the casing. Whilst these stresses locally exceed the yield strength of 450 MPa, the peaks are not a cause for concern, as they represent localised yield over a very small area. Stresses in the fins are largely compressive, reaching values of –372 MPa. There are localised peaks of up to 522 MPa at the point of attachment of the fins to the casing. These area not a cause for concern however, due to their localised nature.

The stresses in the carbon exhibit peak values at the interface between the ends of the long fins and the carbon. This is most likely a result of the way in which contact is modelled between these two surfaces, as well as the limitations of the material model used for the carbon. If these peaks are disregarded, the maximum principal stress in the carbon is 57MPa at the surface immediately below the contact shoes. This relatively high tensile stress is probably due to the steep thermal gradient which exists in the electrode at this point. These high stresses are largely confined to the surface of the electrode, with stresses in the centre of the electrode being compressive. Both Figures 6 and 7 show compressive stresses in a significant proportion of the radius of the baked electrode. This indicates that it is unlikely that cracks caused by these stresses will propagate through the electrode. The material model used for the carbon could not allow for the flow of material in the heated green paste. As a result, stresses obtained in practice are likely to be somewhat lower than those predicted by the model.

In summary, stresses in the region immediately below the contact shoes are significant, both in the steel and the carbon. These high stresses are attributable to the steep thermal gradients experienced in this region. However, as the carbon has already baked at this point, local yielding of the steel should not be a cause for concern. The high tensile stresses on the surface of the carbon attenuate quite rapidly below the contact shoes and in a radial direction.

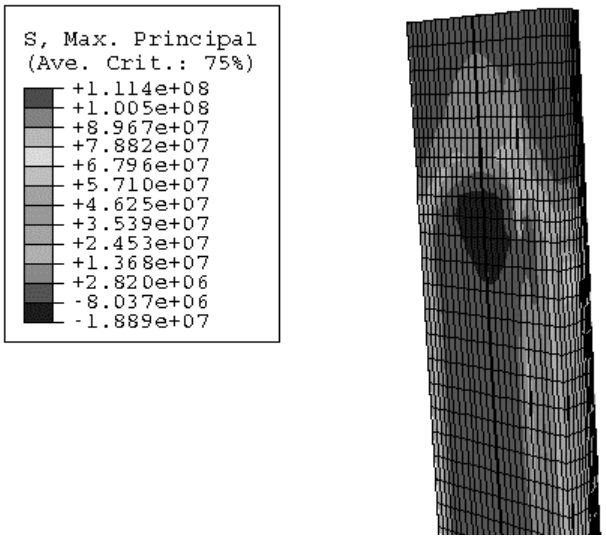

Figure 6. Maximum Principal Stress in Carbon [Pa].

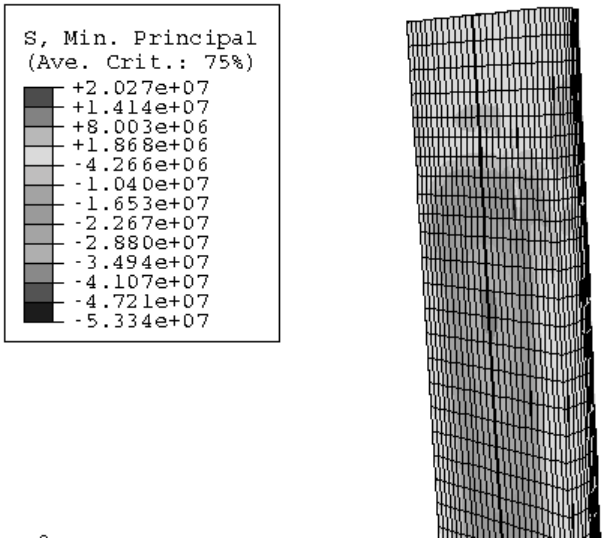

Figure 7. Minimum Principal Stress in Carbon [Pa].

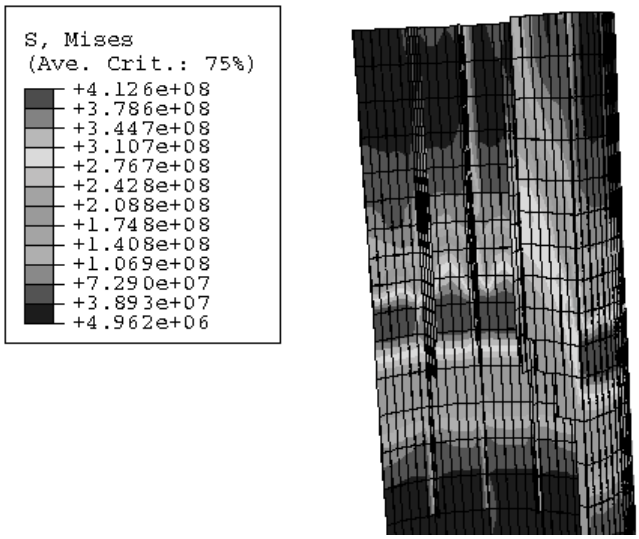

Figure 8. Von Mises Stresses in Steel [Pa.].

4. CONCLUSION

A finite element model of a Søderberg electrode was applied to an evaluation of proposed new casing and fin materials. This study demonstrated the feasibility of using a different material for the casings and fins of the electrodes.

The results of the thermal-stress analysis indicate that the material of construction of both the casing and the fins play a role in determining the position of the critical 450ºC isotherm. The analysis indicates that a casing made from Chromanite with either Grade 304 or Chromanite fins exhibits very similar behaviour to the existing Grade 304 casing and fins.

5. ACKNOWLEDGEMENTS

The authors wish to thank Samancor Chrome and Samancor Manganese for funding this research, and for permission to publish the results.

6. REFERENCES

[1] Olsen, L., Arnesen, A.G., Bencze,I., Innvaer, R., Temperature Distribution in Soderberg Electrodes, Electrowarme Internatinoal 21 (1973)B3, pp 128-131
[2] Innvaer, R., Olsen, L., Temperatures in Soderberg Electrodes in Unsteady State Conditions, 8th Cong of Union Internatinale d' Electrothermie, Liege, 1976
[3] Arensen, A.G., Okstad, S., Innvaer, R., Olsen, L., Operation of Soderberg Electrodes, ILAFA Congress, Acapulco, 1978
[4] Innvaer, R., Olsen, L., Practical Use of Mathematical Models for Soderberg Electrodes
[5] Innvaer, R., Fidje, K., Sira, T., Three Dimensional Calculations on Smelting Electrodes, Electric Furnace Conf Proc, Vol 43, Atlanta Georgia, 1986, pp 265-272.
[6] Innvaer, R., The Soderberg Electrode System – Recent Research and Development – New Challenges, Infacon 89 (Vol 1 1989)
[7] Jonsson, M.T., Ingason, H.T., A Three Dimensional Simulation Model for a Soderberg Electrode, Infacon 8 (1998)
[8] Arai, K., Ono, T. Electrical and Thermal Phenomena in Soderberg Electrodes of Submerged Arc Reduction Furnace Vol , no 1, pp51-63, 1974 (translation) 1
[9] Arai, K., Ono, T. Design Factors affecting the Temperature Distribution in a Soderberg Electrode, Ferroalloys, Vol 24, no 1, pp21-29, 1975 (translation)
[10] Bullon, J., Lage, M., Bermudez, A., Pena, F., The New Compound Electrode: Current Situation and Thermoelectric Studies, Proc Infacon 8
[11] Bermudez, A., Bullon, J., Pena, F. A Finite Element Method for the Thermoelectrical Simulation of Electrodes, Comm. In Numerical Methods in Engineering, 1998, Vol 14, pp 581-593
[12] Bermudez, A., Muniz, M.C., Pena, F. ,Bullon, J., Numerical Computation of the Electromagnetic Field in the Electrodes of a Three-Phase Arc Furnace, Int. Jnl for Numerical Methods in Engineering, 1999, Vol 46, pp 649- 658
[13] Bermudez, A., Bullon, J., Pena, F. ,Salgado, P., A Numerical Method for Transient Simulation of Metallurgical Compound Electrodes, Finite Elements in Analysis and Design, 2003, Vol 39, pp 283-299
[14] Bermudez, A., Rodriguez, R.,Salgado, P. Modelling and Numerical Treatment of Boundary Data in an Eddy Currents Problem, C. R. Acad . Sci. Paris, Ser I 335 (2002) 633-638
[15] Metaxas, A.C., Foundations of Electroheat – A Unified Approach, Wiley, 1996.
[16] ABAQUS, Version 6.3, Hibbett, Karlsson, Sorenson Inc., Rhode Island, http://www.abaqus.com
[17] Innvaer R., Olsen, L., Vatland, A., Operational Parameters for Soderberg Electrodes from Calculations, Measurements and Plant Experience
[18] Larsen, B., Sørlie, M., Ugland, R., High Temperature Properties of Anthracite Based Electrodes